# Prototypal 1,2,3,5-Dithia- and 1,2,3,5-Diselenadiazolyl $[HCN_2E_2]^\bullet$ (E = S, Se): Molecular and Electronic Structures of the Radicals and Their Dimers, by Theory and Experiment

**A. W. Cordes,[1a] C. D. Bryan,[1a] W. M. Davis,[1b] R. H. de Laat,[1b] S. H. Glarum,[1c] J. D. Goddard,[1b] R. C. Haddon,[1c] R. G. Hicks,[1b] D. K. Kennepohl,[1b] R. T. Oakley,*[,1b] S. R. Scott,[1a] and N. P. C. Westwood[1b]**

*Contribution from the Department of Chemistry and Biochemistry, University of Arkansas, Fayetteville, Arkansas 72701, Guelph-Waterloo Centre for Graduate Work in Chemistry, Guelph Campus, Department of Chemistry and Biochemistry, University of Guelph, Guelph, Ontario N1G 2W1, Canada, and AT&T Bell Laboratories, 600 Mountain Avenue, Murray Hill, New Jersey 07974*

*Received February 26, 1993*

**Abstract:** The reactions of *N,N,N'*-tris(trimethylsilyl)formamidine with $ECl_2$ (E = S, Se) afford 1,2,3,5-dithia- and 1,2,3,5-diselenadiazolium chloride, which can be reduced with triphenylantimony to the corresponding dithia- and diselenadiazolyl radicals $[HCN_2E_2]^\bullet$. The solid state structure of the cofacial dimer $[HCN_2S_2]_2$ has been determined by X-ray diffraction; crystals of $[HCN_2S_2]_2$ belong to the monoclinic space group $P2_1/n$, with $a$ = 6.833(6), $b$ = 16.463(4), $c$ = 19.161(4) Å, $\beta$ = 93.57(4)°, $FW$ = 210.30, $Z$ = 12. The crystal structure consists of stacked dimers, with three dimers in the asymmetric unit. Along the stacking axis the mean intradimer S- - -S contact is 3.11 Å; the mean interdimer contact is 3.76 Å. *Ab initio* calculations with split-valence and larger basis sets have been employed to evaluate the structures and energies of both the gas phase radicals and their dimers. Minor changes in geometry are predicted upon association of the monomers; this relative structural invariance is consistent with low binding energies, the best predictions (including zero point vibrational energy corrections) being *ca.* 4 kcal/mol (for E = S) and *ca.* 10 kcal/mol (for E = Se). Theory also provides spin distributions to support the interpretation of the observed ESR parameters (for E = S), confirms the $a_2$ symmetry of the SOMO, yields Koopmans' theorem and ΔSCF ionization potentials for analysis of the PE spectra of the radicals, and furnishes vibrational frequencies and infrared intensities of the sulfur radical. The latter facilitate assignment of the gas-phase IR spectrum.

## Introduction

Interest in the development of molecular conductors based on neutral π-radicals has prompted the study of heterocyclic thiazyl and selenazyl radicals, in particular derivatives of 1,2,3,5-dithia- and 1,2,3,5-diselenadiazolyl $[RCN_2E_2]^\bullet$ (**1**).[2] However, early

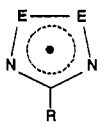


**1**

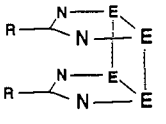


**2**

structural work on a variety of organosubstituted monofunctional sulfur (R = $NMe_2$, Me, Ph, $CF_3$)[3] and selenium (R = Ph)[4] derivatives failed to show the desired stacking of molecular plates. More recently we have investigated the structural consequences of the attachment of cyanofuryl[5] and cyanophenyl[6] groups in the 4-position. As observed elsewhere,[7] the incorporation of the cyano group leads to a solid state packing pattern in which individual molecules are linked by CN- - -E bridges; under favorable circumstances, stacked structures can prevail. Bifunctional[8,9] and trifunctional[10,11] radicals have also been prepared, with the intent of increasing the number and magnitude of close intermolecular E- - -E interactions; the conductivity of these latter systems is certainly improved over those of the monofunctional variants.

Herein we report the preparation of the prototypal heterocycles **1** (R = H). The small size of these radicals has provided an opportunity to examine in detail, by theory and experiment, their electronic and geometric structures, and also the energetics and structural consequences of the dimerization process. To this end we have determined the crystal structure of the dimer **2** of the sulfur radical **1**, which is notably different from that recently communicated for the corresponding selenium derivative.[12] In addition we have characterized the gas phase radicals themselves

(1) (a) University of Arkansas. (b) University of Guelph. (c) AT&T Bell Laboratories.

(2) Cordes, A. W.; Haddon, R. C.; Oakley, R. T. In *The Chemistry of Inorganic Ring Systems*; Steudel, R., Ed.; Elsevier: Amsterdam, The Netherlands, 1992; p 295.

(3) (a) Vegas, A.; Pérez-Salazar, A.; Banister, A. J.; Hey, R. G. *J. Chem. Soc., Dalton Trans.* **1980**, 1812. (b) Hofs, H.-U.; Bats, J. W.; Gleiter, R.; Hartmann, G.; Mews, R.; Eckert-Maksić, M.; Oberhammer, H.; Sheldrick, G. M. *Chem. Ber.* **1985**, *118*, 3781. (c) Cordes, A. W.; Goddard, J. D.; Oakley, R. T.; Westwood, N. P. C. *J. Am. Chem. Soc.* **1989**, *111*, 6147. (d) Banister, A. J.; Hansford, M. I.; Hauptmann, Z. V.; Wait, S. T.; Clegg, W. *J. Chem. Soc., Dalton Trans.* **1989**, 1705.

(4) Del Bel Belluz, P.; Cordes, A. W.; Kristof, E. M.; Kristof, P.; Liblong, S. W.; Oakley, R. T. *J. Am. Chem. Soc.* **1989**, *111*, 9276.

(5) Cordes, A. W.; Chamchoumis, C. M.; Hicks, R. G.; Oakley, R. T.; Young, K. M.; Haddon, R. C. *Can. J. Chem.* **1992**, *70*, 919.

(6) Cordes, A. W.; Haddon, R. C.; Hicks, R. G.; Oakley, R. T.; Palstra, T. T. M. *Inorg. Chem.* **1992**, *31*, 1802.

(7) (a) Suzuki, T.; Fujii, H.; Yamashita, Y.; Kabuto, C.; Tanaka, S.; Harasawa, M.; Mukai, T.; Miyashi, T. *J. Am. Chem. Soc.* **1992**, *114*, 3034. (b) Alcock, N. W. *Adv. Inorg. Radiochem.* **1972**, *15*, 1. (c) Banister, A. J.; Lavender, I.; Rawson, J. M.; Clegg, W. *J. Chem. Soc., Dalton Trans.* **1992**, 859.

(8) Cordes, A. W.; Haddon, R. C.; Oakley, R. T.; Schneemeyer, L. F.; Waszczak, J. V.; Young, K. M.; Zimmerman, N. M. *J. Am. Chem. Soc.* **1991**, *113*, 582.

(9) Andrews, M. P.; Cordes, A. W.; Douglass, D. C.; Fleming, R. M.; Glarum, S. H.; Haddon, R. C.; Marsh, P.; Oakley, R. T.; Palstra, T. T. M.; Schneemeyer, L. F.; Trucks, G. W.; Tycko, R.; Waszczak, J. V.; Young, K. M.; Zimmerman, N. M. *J. Am. Chem. Soc.* **1991**, *113*, 3559.

(10) Cordes, A. W.; Haddon, R. C.; Hicks, R. G.; Oakley, R. T.; Palstra, T. T. M.; Schneemeyer, L. F.; Waszczak, J. V. *J. Am. Chem. Soc.* **1992**, *114*, 1729.

(11) (a) Cordes, A. W.; Haddon, R. C.; Hicks, R. G.; Oakley, R. T.; Palstra, T. T. M.; Schneemeyer, L. F.; Waszczak, J. V. *J. Am. Chem. Soc.* **1992**, *114*, 5000. (b) Cordes, A. W.; Haddon, R. C.; Hicks, R. G.; Kennepohl, D. K.; Oakley, R. T.; Schneemeyer, L. F.; Waszczak, J. V. *Inorg. Chem.* **1993**, *32*, 1554.

0002-7863/93/1515-7232$04.00/0 

Table I. Mean[a] Intramolecular Distances (Å) and Angles (deg) in 2 (R = H; E = S, Se)

| | E = S | E = Se |
|---|---|---|
| E- - -E | 3.11(7) | 3.28(13) |
| E–E | 2.07(3) | 2.326(7) |
| E–N | 1.64(6) | 1.80(3) |
| C–N | 1.32(8) | 1.32(4) |
| C–H | *b* | *b* |
| E–E–N | 95(3) | 91.5(8) |
| E–N–C | 113(5) | 112(2) |
| N–C–N | 124(4) | 134(2) |

[a] The numbers in parentheses are the ranges; in the case of E = S, the average is taken over the three dimers in the asymmetric unit. [b] Idealized H-position (d(C–H) = 0.95 Å).

**Scheme I**

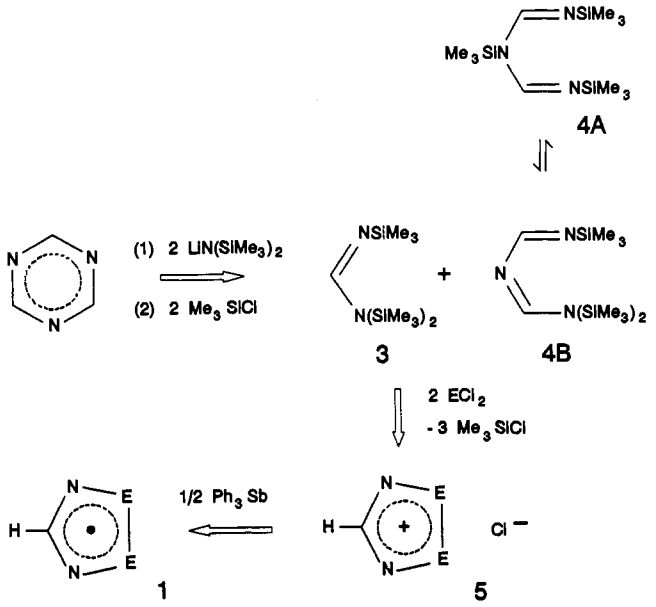


by photoionization mass spectroscopy (PIMS), ultraviolet photoelectron spectroscopy (UPS), and (for E = S) infrared (IR) spectroscopy. Solution and powder pattern electron spin resonance (ESR) spectra on the sulfur radical are also reported. The comprehensive experimental studies are brought into sharper focus by *ab initio* calculations on both the radicals **1** and their dimers **2**.

## Results and Discussion

**Synthesis.** Our primary synthetic route to both 1,2,3,5-dithia- and 1,2,3,5-diselenadiazolium cations has involved the condensation of persilylated amidines $RCN(SiMe_3)_2NSiMe_3$ with $ECl_2$ (E = S, Se). However, the method of preparation of the amidines, the addition of $LiN(SiMe_3)_2$ to a nitrile RCN,[13] appears to be limited to arenenitriles. We have now discovered that the parent compound *N,N,N'*-tris(trimethylsilyl)formamidine (**3**) can be conveniently generated by the reaction of $LiN(SiMe_3)_2{\cdot}Et_2O$ with 1,3,5-triazine, followed by treatment of the intermediate lithiated amidine with trimethylsilyl chloride (Scheme I). The reaction also produces compound **4**;[14] indeed the yield of both products is optimized when the stoichiometry of amide and triazine is 2:1. The dithiadiazolium cation **5** (E = S) can be made in 77% yield by adding **3** slowly to a solution of excess sulfur dichloride in acetonitrile. Reduction of this yellow solid with triphenylantimony in $SO_2$(l) affords **1** (E = S, R = H), which may be purified by slow sublimation at 70 °C/760 Torr (argon) to yield black needles of the corresponding dimer **2**. Addition of **3** to selenium dichloride (prepared *in situ* from Se and $SeCl_4$) in acetonitrile affords the diselenadiazolium cation **5** (E = Se) as a red-brown powder in high yield. Reduction of this crude salt with triphenylantimony in acetonitrile yields 1,2,3,5-diselenadiazolyl (**1**, E = Se, R = H), the dimer of which can be purified by sublimation at 50 °C/$10^{-3}$ Torr as lustrous grey-black needles.

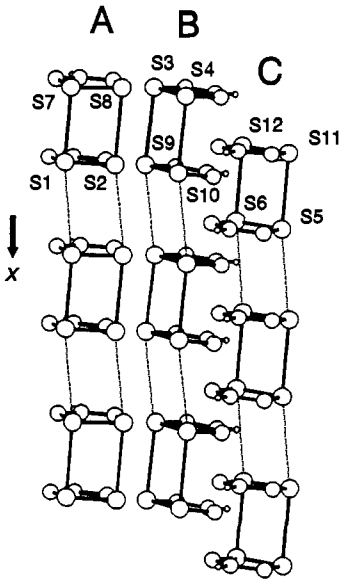


Figure 1. Stacking of dimers within the asymmetric unit of **2** (R = H, E = S).

Table II. Summary of Intra- and Intermolecular S- - -S Distances (Å) in **2** (R = H, E = S)

| Intrastack Contacts | | | |
|---|---|---|---|
| intradimer | | interdimer | |
| S(1)–S(7) | 3.045(7) | S(1)–S(7) at *a* | 3.819(7) |
| S(2)–S(8) | 3.115(7) | S(2)–S(8) at *a* | 3.751(7) |
| S(3)–S(9) | 3.126(6) | S(3)–S(9) at *b* | 3.758(6) |
| S(4)–S(10) | 3.118(6) | S(4)–S(10) at *b* | 3.751(6) |
| S(5)–S(11) | 3.140(7) | S(5)–S(11) at *a* | 3.729(7) |
| S(6)–S(12) | 3.088(7) | S(6)–S(12) at *a* | 3.775(7) |
| Interstack Contacts | | | |
| $d_1$ | S(4)–S(6) at *b* | | 3.690(6) |
| $d_2$ | S(4)–S(12) | | 3.483(5) |
| $d_3$ | S(6)–S(10) | | 3.500(5) |
| $d_4$ | S(10)–S(12) | | 3.542(6) |
| $d_5$ | S(3)–S(9) at *c* | | 3.352(6) |
| $d_6$ | S(9)–S(9) at *c* | | 3.441(8) |
| $d_7$ | S(4)–S(8) | | 3.515(5) |
| $d_8$ | S(2)–S(10) | | 3.498(5) |

*a* $-1+x, y, z$
*b* $1+x, y, z$
*c* $1-x, 2-y, 1-z$

**Crystal and Molecular Structure of 2 (E = S, R = H).** The crystal structure (triclinic, space group $P\bar{1}$) of the dimer **2** of the selenium-based radical **1** (E = Se, R = H) was described in an earlier communication.[12] A summary of intramolecular structural parameters is provided in Table I. Crystals of the dimer of **1** (E = S, R = H) belong to the monoclinic space group $P2_1/n$, and while this structure also consists of cofacial dimers **2**, the molecular units are packed in a fashion which differs markedly from that found for the selenium compound. There are three dimers (designated **A**, **B**, and **C**) in the asymmetric unit, each of which forms slightly slipped stacks running parallel to *x* (Figure 1).

(12) Cordes, A. W.; Glarum, S. H.; Haddon, R. C.; Hallford, R.; Hicks, R. G.; Kennepohl, D. K.; Oakley, R. T.; Palstra, T. T. M.; Scott, S. R. *J. Chem. Soc., Chem. Commun.* **1992**, 1265.

(13) Boeré, R. T.; Oakley, R. T.; Reed, R. W. *J. Organomet. Chem.* **1987**, *331*, 161.

(14) The *N,N',N''*-tris(trimethylsilyl)-1,3,5-triaza-1,4-pentadiene (**4**) can exist in several tautomeric forms. In benzene solution, isomer A dominates, while in chloroform isomers A and B are both observed.

Table III. *Ab Initio* Total Energies (hartrees) and Binding Energies (kcal mol$^{-1}$) for **1** and **2** (R = H; E = S, Se)[a]

| | total energies | | | | binding energies with ZPVE correction | |
|---|---|---|---|---|---|---|
| | LANL1DZ* | | 3-21G* | | | |
| | **1** | **2** | **1** | **2** | LANL1DZ* | 3-21G* |
| | | | E = S | | | |
| HF | −167.065 05 | −334.029 16 | −937.791 05 | −1875.485 94 | −60.04 | −56.97 |
| MP2 | −167.578 51 | −335.220 15 | −938.308 85 | −1876.679 14 | +42.63 | +41.92 |
| MP3 | −167.600 99 | −335.209 08 | −938.330 01 | −1876.664 90 | +7.76 | +6.43 |
| MP4SDQ | −167.620 50 | −335.241 74 | −938.349 31 | −1876.699 68 | +3.76 | +4.03 |
| | | | E = Se | | | |
| HF | −165.307 10 | −330.519 08 | −4923.861 59 | −9847.655 04 | −56.99 | −39.64 |
| MP2 | −165.798 18 | −331.676 81 | −4924.385 70 | −9848.873 68 | +53.18 | +67.30 |
| MP3 | −165.816 53 | −331.646 16 | −4924.400 14 | | +10.92 | |
| MP4SDQ | −165.837 63 | −331.686 69 | −4924.420 58 | | +9.87 | |

[a] A positive sign for the binding energy implies that the dimer is bound.

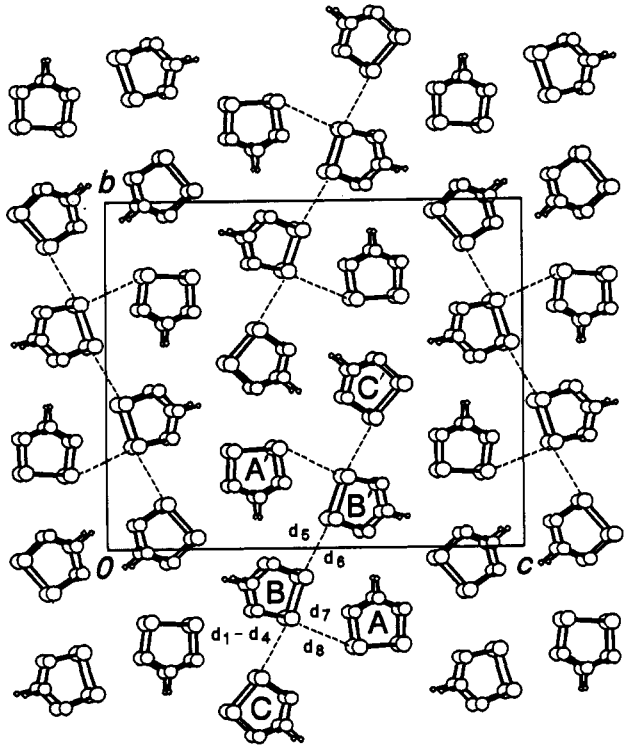


**Figure 2.** Packing of **2** (R = H, E = S) viewed down the *x* axis.

Intra- (mean value 3.11 Å) and interdimer (mean value 3.76 Å) S- - -S contacts along the stacks (Table II) are similar to those seen in related stacked structures.[5,6,9,11] The packing of the stacked dimer columns, *i.e.*, the view down the *x* axis, is illustrated in Figure 2. There is a series of strong intercolumnar S- - -S interactions within the asymmetric unit (see Table II) which connect the B and C columns ($d_1$–$d_4$) and the **B** and **A** columns ($d_7$ and $d_8$). There are also close interactions between **B** and **B'** columns ($d_5$ and $d_6$) across an inversion center. Collectively these contacts knit the columns into centrosymmetric clusters of six (two asymmetric units). Although there are contacts between these clusters, they are all greater than 3.9 Å.

***Ab Initio* Calculations.** The theoretical portion of this study establishes a computational model (especially with regard to the basis set) necessary to predict accurately the properties and structures of the prototypal dithia- and diselenadiazolyl radicals (**1**, R = H). In addition, theoretical studies of the dimers **2** provide the first step toward understanding the associated dimers in the solid state. There is little or no experimental data on the dimer *per se* (*i.e.*, free from lattice forces in the solid), but knowledge of the changes in structure upon association of the radicals and the binding energies predicted by reliable theory are of value in understanding the chemistry and physics of these systems.

Table IV. Calculated Distances (Å) and Angles (deg) for **1** and **2** (R = H, E = S)

| | LANL1DZ* | CEP31G* | 3-21G* | 6-31G* | 6-31G** |
|---|---|---|---|---|---|
| | | | **1** (R = H, E = S) | | |
| d(S–S) | 2.121 | 2.100 | 2.125 | 2.092 | 2.092 |
| d(S–N) | 1.659 | 1.660 | 1.660 | 1.652 | 1.652 |
| d(C–H) | 1.351 | 1.340 | 1.344 | 1.327 | 1.327 |
| d(C–N) | 1.066 | 1.080 | 1.065 | 1.072 | 1.073 |
| (S–S–N) | 94.0 | 94.6 | 94.4 | 94.5 | 94.3 |
| (S–N–C) | 115.5 | 113.3 | 115.3 | 113.8 | 113.9 |
| (N–C–N) | 129.0 | 124.2 | 121.8 | 123.8 | 123.6 |
| | | | **2** (R = H, E = S) | | |
| d(S- - -S) | 3.154 | | 3.026 | | |
| d(S–S) | 2.075 | | 2.071 | | |
| d(S–N) | 1.639 | | 1.635 | | |
| d(C–N) | 1.332 | | 1.323 | | |
| d(C–H) | 1.066 | | 1.065 | | |
| (S–S–N) | 94.5 | | 94.4 | | |
| (S–N–C) | 114.5 | | 114.2 | | |
| (N–C–N) | 122.0 | | 122.6 | | |

Firstly, it should be stated that only the most reliable results are presented in this work. Following some experimentation with minimal basis sets, it was apparent that at least a split-valence basis set with additional d functions on sulfur or selenium would be required, *i.e.*, 3-21G*. For example, valence minimal basis sets gave large distortions to lower symmetry structures for the dimers which appeared to maximize N–N rather than S–S or Se–Se inter-ring bonding. Thus a split-valence basis set was used for both the monomers and dimers. In order to reduce the computational burden further, two different effective core potentials were also employed, with split-valence basis sets and d functions added, *i.e.*, LANL1DZ* and CEP31G*. The LANL1DZ basis was supplemented by a set of six d functions on S and Se only, while the CEP31G was augmented with such d functions on C and N as well. The core potentials for Se were parametrized using relativistic atomic SCF results. In the case of the dithiadiazolyl radical, for which more experimental data is available (*e.g.*, the gas-phase IR spectrum), numerical predictions were made with larger all-electron basis sets, 6-31G* and 6-31G**. Most comparisons with experiment are based on the 3-21G* basis set, although the vibrational spectrum of the sulfur radical has been considered at the 6-31G** level. The total energies for both S and Se radicals and their respective dimers are given in Table III.

With respect to the calculated structures, the agreement between the various basis sets (and, indeed, experiment) for the radicals is very good. Tables IV and V present the UHF optimized geometries of the dithia- and diselenadiazolyl radicals. For the sulfur compound, all basis sets predict distances of 2.1 Å (S–S), 1.65–1.66 Å (S–N), and 1.33–1.35 Å (C–N). These values are close to those (*ca.* 2.06, 1.64, and 1.33 Å, respectively) observed in the crystal structure of **2** (R = H, E = S). The SSN and SNC bond angles of *ca.* 94 and 114° are also in very good agreement

Table V. Calculated Distances (Å) and Angles (deg) for 1 and 2 (R = H, E = Se)

| | LANL1DZ* | CEP31G* | 3-21G* |
|---|---|---|---|
| | 1 (R = H, E = Se) | | |
| d(Se–Se) | 2.388 | 2.354 | 2.352 |
| d(Se–N) | 1.811 | 1.798 | 1.830 |
| d(C–N) | 1.352 | 1.341 | 1.343 |
| d(C–H) | 1.070 | 1.083 | 1.075 |
| (Se–Se–N) | 90.1 | 90.8 | 90.8 |
| (Se–N–C) | 117.5 | 115.5 | 116.0 |
| (N–C–N) | 124.8 | 127.4 | 126.6 |
| | 2 (R = H, E = Se) | | |
| d(Se- - -Se) | 3.311 | | 3.072 |
| d(Se–Se) | 2.323 | | 2.269 |
| d(Se–N) | 1.780 | | 1.803 |
| d(C–N) | 1.332 | | 1.322 |
| d(C–H) | 1.070 | | 1.076 |
| (Se–Se–N) | 90.9 | | 91.8 |
| (Se–N–C) | 115.9 | | 113.7 |
| (N–C–N) | 116.4 | | 129.0 |

with the X-ray diffraction analysis (Table I) presented above. For the selenium radical the predicted distances are 2.35 Å (Se–Se), 1.80–1.83 Å (Se–N), and 1.34 Å (C–N), values which again agree quite closely with the corresponding mean experimental intramolecular distances listed in Table I. This agreement is satisfying, not so much in a quantitative sense but rather for the support it gives to our premise of very limited electronic changes upon dimerization and packing in the solid state. Although spin contamination in the UHF treatment of the radicals might have been expected to have geometrical consequences, the major effect as revealed by ROHF studies is to shorten the distances in the rings slightly, *e.g.*, the C–N distance decreases from 1.33 to 1.32 Å in the dithiadiazolyl radical.

The theoretical structures of the sulfur and selenium dimers are also summarized in Tables IV and V. As the E–N antibonding $a_2$ singly occupied molecular orbital (SOMO) **6** of the radicals

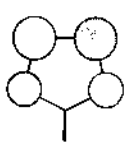

**6**

is involved in the dimerization, the individual rings have reduced antibonding upon dimerization. The S–N or Se–N distance shortens slightly, as do the intramolecular S–S and Se–Se bond lengths. The distance between the rings is predicted to be between 3.0 and 3.2 Å for the sulfur and between 3.1 and 3.3 Å for the selenium case. Both values are in good agreement with the experimental results in Table I. From theory both monomers retain their essential structure upon dimerization, and a comparison of theory and experiment shows that the dimers maintain their essence within the extended solid state structures. It is of interest that the interannular Se–Se distance is nearly the same as that of the S–S both experimentally and theoretically, despite the differences in van der Waals radii[15] (S, 1.80, and Se, 1.90 Å). The closer approach of the selenium rings relative to the sum of the nonbonded radii may be taken as indicative of a stronger interaction in this species relative to the sulfur analog. The calculated energetics of dimerization of the radicals proved to be very sensitive to the method employed (see Table III). For a radical combination reaction, the SCF approach is not quantitatively accurate and electron correlation effects were therefore included. At low order of perturbation theory (MP2) the sulfur dimer is bound by *ca.* 42 kcal/mol and the selenium dimer by a larger amount, *ca.* 60 kcal/mol; these binding energies include changes in zero point vibrational energy between the two radicals and the dimer. However, when the calculations are extended to third (MP3) and partial fourth (MP4SDQ) order, the binding energies change to *ca.* 6.4 and 4.0 kcal/mol (with ZPVE correction) for the sulfur species. These results may be compared with the experimental value of 8 kcal/mol determined (by solution ESR methods) for the corresponding phenyl derivative.[16] For the selenium compound, computer resources were only sufficient to determine the MP3 and MP4SDQ energies using the LANL1DZ* basis set. The calculated binding energies using this basis set were *ca.* 10.9 (MP3) and 9.9 kcal/mol (MP4SDQ). Comparing these results with the LANL1*DZ** and 3-21G* results on the sulfur dimer, the binding energies of the selenium species using the 3-21G* basis set are anticipated to be in the neighborhood of 10 kcal/mol. The calculations thus confirm that the selenium dimer is more strongly bound than the sulfur, as suggested by the interannular distances in the dimers and by the temperature dependence of the ESR signal intensity (*vide infra*). Similar conclusions have been reached for related radical systems.[17] The small binding energies of both dimers are also consistent with the limited structural changes observed upon association of the monomers.

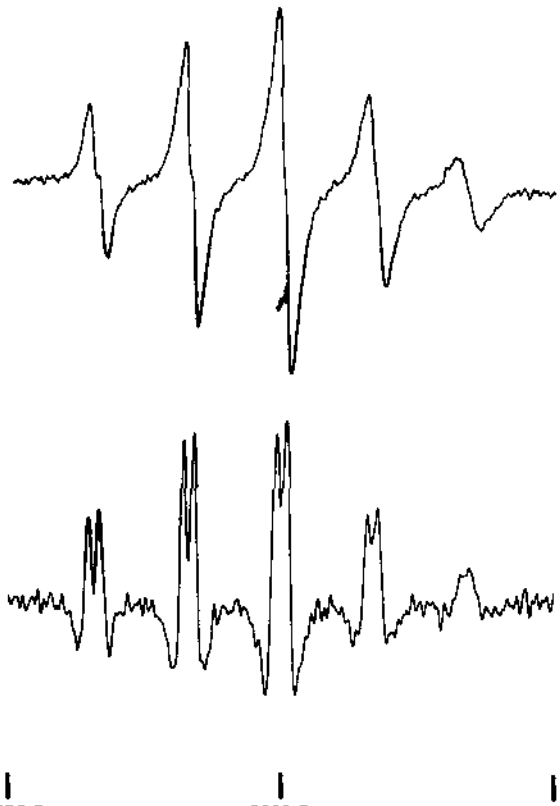


Figure 3. ESR spectrum of 1 (R = H, E = S) in toluene at 169 K. The upper plot is the first derivative; the lower plot is the second derivative.

**ESR Spectra.** The solution ESR spectrum of $[HCN_2Se_2]^{\bullet}$ in $CH_2Cl_2$ was reported earlier.[2] Variable-temperature studies on this species afforded some line-narrowing at lower temperatures, but further resolution of the broad singlet could not be achieved. At about −80 °C the signal disappeared, presumably as a result of dimerization of the radicals. We have had more success with the sulfur derivative; at room temperature the ESR spectrum of $[HCN_2S_2]^{\bullet}$ in toluene consists of a poorly resolved quintet at $g$ = 2.0102. The low resolution presumably arises from the small size of the radical and the expected rapid rotational relaxation.

(15) Bondi, A. *J. Phys. Chem.* **1964**, *68*, 441.

(16) Fairhurst, S. A.; Johnson, K. M.; Sutcliffe, L. H.; Preston, K. F.; Banister, A. J.; Hauptman, Z. V.; Passmore, J. *J. Chem. Soc., Dalton Trans.* **1986**, 1465.

(17) The stronger association of selenium- vs sulfur-based heterocyclic radicals has been measured for other systems. See, for example: Oakley, R. T.; Reed, R. W.; Cordes, A. W.; Craig, S. L.; Graham, J. B. *J. Am. Chem. Soc.* **1987**, *109*, 7745.

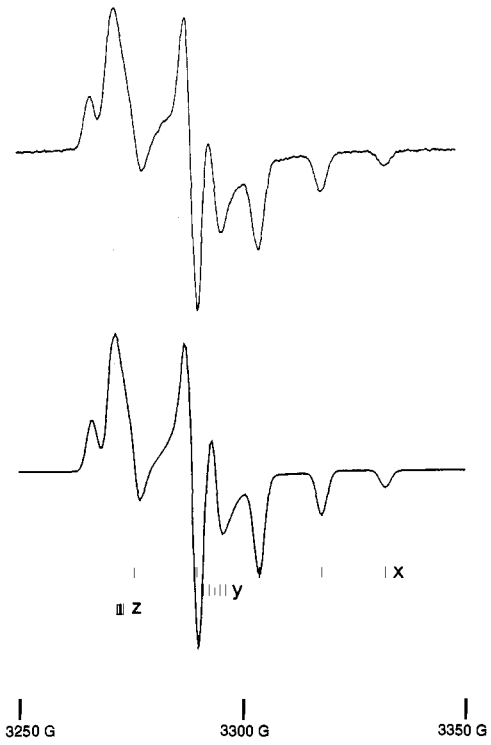


**Figure 4.** Powder pattern ESR spectrum of **1** (R = H, E = S) at 66 K. The upper plot is the observed spectrum, while the lower is a computer simulation (see Table VI).

**Table VI.** Anisotropic $g$ and $a_N$ (mT) Values ESR Parameters for **1** (E = S)

| | R = H | | R = Me[a] | | R = Ph[a] | |
|---|---|---|---|---|---|---|
| | $g$ | $a_N$ | $g$ | $a_N$ | $g$ | $a_N$ |
| $xx$ | 2.0018 | 1.41 | 2.0026 | 1.43 | 2.0021 | 1.410 |
| $yy$ | 2.0080 | 0.12 | 2.0090 | 0.08 | 2.0078 | 0.107 |
| $zz$ | 2.0210 | 0.035 | 2.0215 | 0.11 | 2.0218 | 0.035 |

[a] From ref 16.

When the solution is cooled to 169 K, the resolution improves, and analysis of the second-derivative spectrum reveals a quintet of doublets (Figure 3), from which we assign the anisotropic hyperfine coupling parameters $a_N$ = 0.508 mT and $a_H$ = 0.055 mT. The near invariance of the ESR signal intensity with temperature for the sulfur radical supports the notion of a binding energy close to zero, whereas the collapse of the ESR signal intensity of the selenium species at lower temperatures suggests a more exothermic dimerization enthalpy.

A reasonably well-resolved powder pattern ESR spectrum of $[HCN_2S_2]^\bullet$ was obtained by examining a frozen solution of the radical in toluene at 66 K (Figure 4). Computer simulation of this spectrum afforded anisotropic g and $a_N$ parameters (Table VI) very similar to those reported earlier for the corresponding methyl and phenyl derivatives **1** (E = S, R = Me and Ph).[16] The marked anisotropy in the $a$-values is consistent with a $\pi$-radical. The *ab initio* predicted spin distributions of both the sulfur and selenium radicals were examined at the 3-21G* UHF level; the diagonal elements of the spin density matrices were H 0.04, C −0.76, N 0.91, and S 0.21 for the sulfur and H 0.05, C −0.76, N 0.94, and Se 0.09 for the selenium derivatives. These values are consistent with our previous results on thia- and selenatriazinyls and suggest a greater tendency for selenium (which is less electronegative than sulfur) to shed spin density onto nitrogen.[18] The Fermi contact terms (in atomic units) are H 0.015, C −0.148, N 0.194, and S 0.030 in the dithia species as compared to H 0.016, C −0.155, N 0.197, and Se −0.002 in the diselena species.

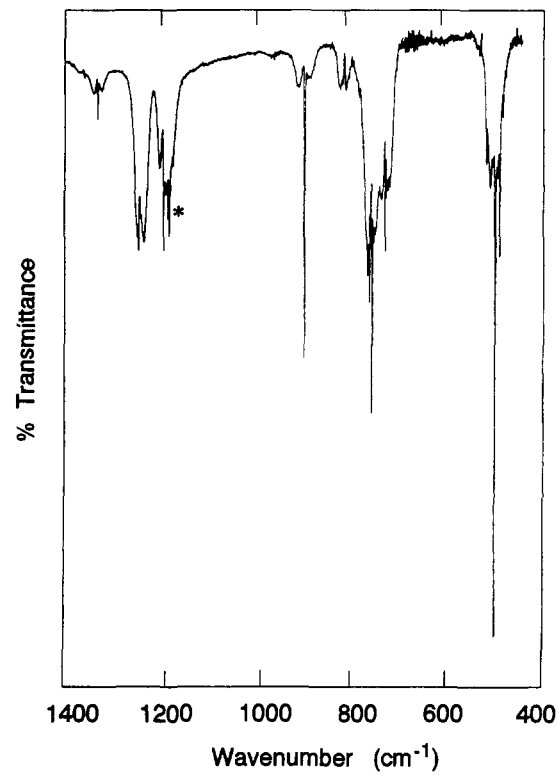


**Figure 5.** Gas-phase infrared spectrum of **1** (R = H, E = S), 400–1400 $cm^{-1}$. The sharp feature marked with an asterisk is an unknown impurity.

**Infrared Spectra.** The major peaks from the Nujol mull IR spectra of **2** (R = H) are summarized in the Experimental Section. The vibrational frequencies correspond, of course, to the dimers rather than the radicals themselves, and the strong interdimer interactions in the Se compound may well influence some of the intramolecular modes. SCF level (3-21G* basis set) vibrational frequencies were determined for the cations **5**, radicals **1**, and dimers **2**. In most cases the strong or very strong bands observed in the Nujol mulls for the cations and dimers could be qualitatively assigned with reference to the theoretical spectra.

While the selenium compound is insufficiently volatile for gas phase measurements, the vapor pressure of $[HCN_2S_2]^\bullet$, about 200 mTorr at room temperature, has allowed us to examine the IR spectrum of the discrete radical. This molecule is an oblate asymmetric rotor ($\kappa_{calc}$ = 0.48) and has 12 vibrational degrees of freedom which transform (in $C_{2v}$) as $5A_1 + A_2 + 2B_1 + 4B_2$. All are infrared active except the $A_2$ mode. The $A_1$, $B_1$, and $B_2$ fundamentals give respectively B-, C-, and A-type bands, since the $a$-axis lies perpendicular to the $C_2$ axis. Nine of these modes are seen between 4000 and 400 $cm^{-1}$. Figure 5 shows the gas-phase IR spectrum of $[HCN_2S_2]^\bullet$ between 400 and 1400 $cm^{-1}$. With calculated (6-31G**) rotational constants of $A$ = 5.4251 GHz, $B$ = 4.6659 GHz, and $C$ = 2.5085 GHz, the calculated PR separations of the A-, C-, and B-type bands are 17.2, 17.2, and 25.9 $cm^{-1}$, respectively, in good agreement with experiment. In general (but see below), the band contours provide reasonably unambiguous assignment of the bands, and this is supported by the calculated (*ab initio*, 6-31G**) frequencies (scaled by 0.90 to partially correct for anharmonicity and the SCF approximation) and the calculated intensities which are also included in Table VII together with the band types and proposed assignments. The two C-type bands at 900 and 500 $cm^{-1}$, corresponding to the $\nu_7$ and $\nu_8$ fundamentals, are classic examples of their genre and are computed within 23 $cm^{-1}$ of their experimental positions. Of the four A-type bands ($\nu_9$, $\nu_{10}$, $\nu_{11}$, and $\nu_{12}$), the first three are quite unambiguous according to their rotational profiles. The spike

(18) Bestari, K.; Cordes, A. W.; Oakley, R. T.; Young, K. M. *J. Am. Chem. Soc.* **1990**, *112*, 2249.

**Table VII.** Observed and Calculated (6-31G**)[a] Infrared Wavenumbers ($cm^{-1}$) for **1** (R = H, E = S)

| observed | | calculated | | symmetry |
|---|---|---|---|---|
| freq | band type | freq | intensity[b] | and assignment |
| | | 219 | 0 | $A_2$ ($\nu_6$) |
| | | 475 | 0.1 | $A_1$ ($\nu_5$) |
| 489[c] | A | 494 | 11 | $B_2$ ($\nu_{12}$) |
| 500 | C | 478 | 27 | $B_1$ ($\nu_8$) |
| 729 | B | 698 | 11 | $A_1$ ($\nu_4$) |
| 757 | A | 719 | 54 | $B_2$ ($\nu_{11}$) |
| 815 | B | 815 | 1.3 | $A_1$ ($\nu_3$) |
| 900 | C | 877 | 6.4 | $B_1$ ($\nu_7$) |
| 1196 | A | 1108 | 1.4 | $B_2$ ($\nu_{10}$) |
| 1243 | B | 1206 | 33 | $A_1$ ($\nu_2$) |
| 1333 | A | 1326 | 0.5 | $B_2$ ($\nu_9$) |
| | | 3060 | 5.7 | $A_1$ ($\nu_1$) |

[a] UHF, scaled by 0.90. [b] Theoretical intensities in km/mol. [c] This band is partially obscured by the strong band at 500 $cm^{-1}$.

(asterisk) at 1185 $cm^{-1}$ on the P-branch of $\nu_{10}$ is an unknown impurity whose intensity fluctuates with time. The lowest observable A-type, $\nu_{12}$, is partly obscured by the strong C-type at 500 $cm^{-1}$; without the benefit of higher resolution, we assign it tentatively to the feature at 489 $cm^{-1}$, although calculation places it to the high-wavenumber side of the C-type band. The $\nu_1$ fundamental (predicted at 3060 $cm^{-1}$) is not observed, since $(\partial\mu/\partial Q_1)_0$ is small, and the interferometer loses some sensitivity in this region. Two of the B-type bands are clearly identified from their profiles at 1243 ($\nu_2$) and 815 ($\nu_3$) $cm^{-1}$. The remaining B-type ($\nu_4$) is placed at 729 $cm^{-1}$, albeit with a more unclear rotational profile. The average discrepancy between experiment and theory is 28 $cm^{-1}$, and the excellent correspondence, including the calculated intensities, provides satisfying confirmation that the equilibrium gas-phase species above the solid is uniquely the radical; there is no evidence for a gas-phase dimer.

**Photoionization Mass Spectra and UV Photoelectron Spectra.** HeI ultraviolet photoelectron spectra of **1** (R = H; E = S, Se) have been obtained by vaporization of the radical dimers. The data indicate the presence of monomeric gas-phase radicals, and this was confirmed by using PIMS whereby the concomitant ion was extracted into an *in situ* quadrupole mass analyzer (Hiden Analytical Ltd.). The extent of fragmentation could be controlled by using either HeI (21.22 eV) or unfiltered $HL_\alpha$ (95% 10.2 eV) radiation. The parent monomer ions ($m/e$ = 105 (S) and 201 (Se)) were the dominant species with $HL_\alpha$.

The PE spectra (Figure 6) show a single discrete low ionization energy (IE) corresponding to the $a_2$ SOMO **6**. Interestingly, the values for the first IEs are very similar, 7.87 and 7.71 eV for E = S and Se, respectively, but the observed trend is certainly in keeping with the expected electronegativity differences. Similar differences, in sense and magnitude, were observed for the redox potentials of the corresponding R = Ph derivatives.[4] In the case of E = S, the values are not far shifted from those of the $CF_3$-, Cl-, and Ph-substituted compounds (the SOMO is nodal at carbon),[19] whereas higher IEs in the Se compounds are shifted by as much as 1 eV lower. Experimental and theoretical (3-21G*) values are given in Table VIII. It should be noted that other basis sets show little variation in the computed IEs. The ΔSCF values confirm the similarity of the first IEs for the S and Se compounds with calculated values of 8.52 and 8.30 eV, respectively, whereas higher IEs, whether Koopmans' or ΔSCF, show a much larger shift, tracking those observed experimentally.

Earlier work involving substituted radicals indicated that the region above 10 eV leading up to the lowest $b_1(\pi)$ orbital should contain five or six in- and out-of-plane ring orbitals in addition to ligand-based orbitals. The parent H-substituted species permits a clearer view of these ring orbitals, with distinct groups of peaks

(19) Boeré, R. T.; Oakley, R. T.; Reed, R. W.; Westwood, N. P. C. *J. Am. Chem. Soc.* **1989**, *111*, 1180.

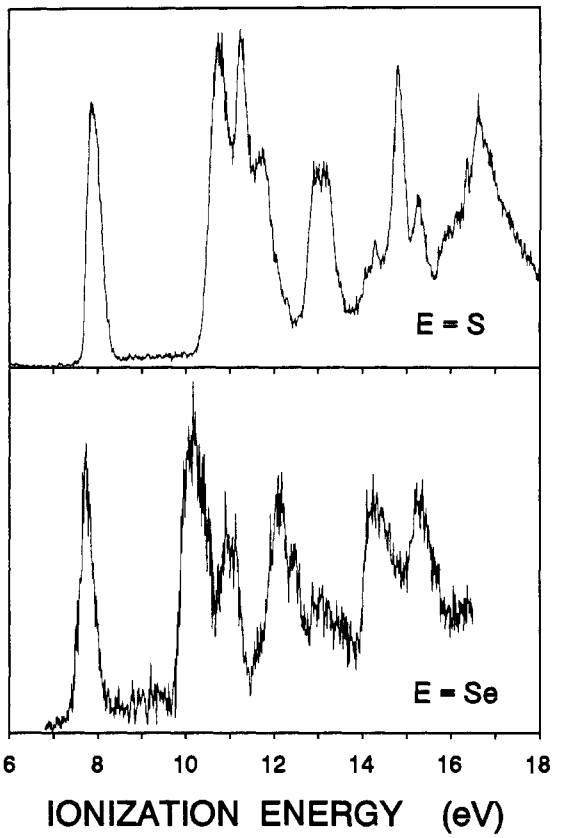


**Figure 6.** Ultraviolet photoelectron spectra of **1** (R = H; E = S, Se).

**Table VIII.** Observed and Calculated (3-21G*) Vertical IEs (eV) for **1** (R = H; E = S, Se)

| observed[a] | orbital | Koopmans' IE[b] | ΔSCF (state) |
|---|---|---|---|
| | **1** (R = H, E = S) | | |
| 7.87 | $a_2(\pi)$ | 8.27 | 8.52 ($^1A_1$) |
| 10.68 | $b_1(\pi)$ | 11.41 | 10.44 ($^3B_2$) |
| 11.18 | $a_1(\sigma)$ | 11.59 | 11.15 ($^3A_2$) |
| 11.65 | $b_2(\sigma)$ | 12.59 | 10.52 ($^3B_1$) |
| 12.92 | $a_1(\sigma)$ | 13.46 | |
| 12.92 | $a_2(\pi)$ | 13.69 | |
| 14.2 | $b_2(\sigma)$ | 15.28 | |
| 14.67 | $b_1(\pi)$ | 16.34 | |
| 16.49 | $a_1(\sigma)$ | 17.67 | |
| | **1** (R = H, E = Se) | | |
| 7.71 | $a_2(\pi)$ | 7.72 | 8.30 ($^1A_1$) |
| 10.1 | $b_1(\pi)$ | 10.46 | 9.77 ($^3B_2$) |
| 10.1 | $a_1(\sigma)$ | 10.85 | 10.58 ($^3A_2$) |
| 11.00 | $b_2(\sigma)$ | 11.48 | 9.67 ($^3B_1$) |
| 12.19 | $a_1(\sigma)$ | 12.32 | |
| 12.19 | $a_2(\pi)$ | 12.95 | |
| 13.1 | $b_2(\sigma)$ | 14.73 | |
| 14.3 | $b_1(\pi)$ | 15.51 | |
| 15.2 | $a_1(\sigma)$ | 16.84 | |

[a] Experimental IEs are ±0.03 eV, unless otherwise indicated. [b] Koopmans' IEs were scaled by 0.92.

based at *ca.* 11, 13, and 15 eV in $[HCN_2S_2]^\bullet$. Although we have not explicitly calculated all of the ionic states, a Koopmans' based approach (assuming negligible triplet/singlet splitting), which does not strictly hold for open shell systems, has been shown to work reasonably well for such radicals[19] and gives plausible groupings of molecular orbitals, although within a particular group a definitive assignment is not feasible.[20] The scaled 3-21G* values for $[HCN_2S_2]^\bullet$ indicate a proposed assignment of $b_1(\pi)$, $a_1$, and $b_2$ ring orbitals for the tight grouping of three peaks at 10.68,

(20) It should be noted that the MNDO method used previously (ref 19) preferentially destabilized the deeper $a_2$ and $b_1$ orbitals. This is attributed to the parametrization for sulfur permitting a shorter S–S bond (calc MNDO 1.96 Å, compared to experiment 2.07 Å).

11.18, and 11.65 eV. ΔSCF calculations for the corresponding ionic states (Table VIII) show a similar grouping, albeit with a different ordering from the Koopmans' calculations. A similar cluster is observed (and calculated, 3-21G* SCF) for $[HCN_2Se_2]^{\bullet}$, shifted by some 0.6 eV to lower IE and exhibiting a coalescence of the first pair of peaks. The broad band centered at 12.92 eV in $[HCN_2S_2]^{\bullet}$ is assigned to the closely spaced $a_1$ and $a_2(\pi)$ orbitals (calculated to be within 0.23 eV); the analogous band in the selenium radical occurs at 12.19 eV. The prominent peak at 14.67 eV in $[HCN_2S_2]^{\bullet}$, observed also in the $CF_3$- and Cl-substituted species,[19] is associated with the lowest (and bonding) $\pi$ level ($b_1$). The position of the $b_2$ orbital is rather more problematic with low-intensity bands observed to both low- and high-IE sides of the sharp 14.67-eV peak. These may involve weak singlet states, and/or multielectron satellites (a common feature of S-containing species).[21] A proposed, but not definitive, assignment in this region follows the calculations and assigns the $b_2$ orbital in $[HCN_2S_2]^{\bullet}$ to the weak band at 14.2 eV. In the selenium analog these bands appear to be more spread out, with the $b_2$ and $b_1$ orbitals at 13.1 and 14.3 eV, respectively. The calculations indicate one additional orbital in the HeI energy range, the $a_1$, observed at 16.49 and 15.2 eV for $[HCN_2S_2]^{\bullet}$ and $[HCN_2Se_2]^{\bullet}$, respectively. The weak peak at 15.1 eV in the S analog is attributed to either the singlet version of the 14.67 eV band or a shake-up satellite.

## Summary

This study on the prototypal radicals **1** and dimers **2** has provided extensive results on both gaseous and solid state structures. The weakness of the dimer units, as indicated by the ESR spectra (for E = S), the ability to produce gas phase monomeric radicals (PIMS, UPS, FTIR), and the lack of structural reorganization upon dissociation are fully supported by the computed monomer and dimer structures. Both experiment (ESR) and theory indicate a slightly stronger interaction in the case of the selenium species; the *ab initio* dimer binding energies are 4 kcal/mol for sulfur and approximately 10 kcal/mol for selenium. An additional novelty of this work is the generation of gaseous radicals, for which PIMS and UPS data can be obtained. The first IEs for the two radicals are similar, although slightly lower in the case of E = Se. Calculated and experimental vibrational spectra of the more volatile sulfur-based radical are in good agreement, and the assignments are supported by the rotational band envelopes.

## Experimental Section

**Starting Materials and General Procedures.** 1,3,5-Triazine, lithium bis(trimethylsilyl)amide, sulfur dichloride, selenium powder, and triphenylantimony were all obtained commercially (Aldrich); sulfur dioxide was obtained from Matheson and used as received. Sulfur dichloride was distilled before use, and $LiN(SiMe_3)_2$ was converted into its diethyl etherate in order to facilitate amidine synthesis.[13] Selenium tetrachloride was prepared according to literature methods.[22] Methylene chloride (Fisher) and acetonitrile (Fisher HPLC grade) were purified by distillation from $P_2O_5$. All reactions were performed under an atmosphere of nitrogen. EI mass spectra were recorded on a Kratos MS890 mass spectrometer. $^1H$ NMR spectra were recorded at 200 MHz on a Varian Gemini 200 spectrometer. Elemental analyses were performed by MHW laboratories, Phoenix, AZ.

**Reaction of *s*-Triazine with 2 equiv of $LiN(SiMe_3)_2{\cdot}Et_2O$.** A solution of 1,3,5-triazine (9.38 g, 0.116 mol) in 80 mL of toluene was added slowly (dropping funnel) to a slurry of $LiN(SiMe_3)_2{\cdot}Et_2O$ (57.6 g, 0.24 mol) in 150 mL of toluene. The mixture was heated gently (50 °C) for 10 h to give a pale golden brown solution. The solution was cooled to room temperature, a solution of trimethylsilyl chloride (30.0 g, 0.28 mol) in 50 mL of toluene was added (dropping funnel), and the reaction was gently refluxed for 16 h. After being cooled to room temperature, the mixture was filtered to remove the lithium chloride precipitate, and the toluene was removed by vacuum distillation. Slow vacuum distillation of the brown oily liquid produced *N,N,N'*-tris(trimethylsilyl)formamidine, yield 24.0 g (80%), bp 35 °C/$10^{-2}$ Torr. $^1H$ NMR δ ($CDCl_3$) 7.96 (s, 1H, *H*C), 0.16 (s, 27H, $Me_3Si$). Anal. Calcd for $C_{10}H_{28}N_3Si_3$: C, 46.09; H, 10.83; N, 10.75. Found: C, 46.08; H, 10.65; N, 10.93. The solid residue from the distillation was vacuum-sublimed at 55 °C/$10^{-2}$ Torr to give *N,N',N''*-tris(trimethylsilyl)-1,3,5-triaza-1,4-pentadiene (**4**) as moisture-sensitive white needles, yield 24.7 g (74%), mp 58–60 °C. Anal. Calcd for $C_{11}H_{29}N_3Si_3$: C, 45.94; H, 10.46; N, 14.61. Found: C, 45.73; H, 10.47; N, 14.66. $^1H$ NMR ($C_6D_6$) δ (ppm) 8.72 (s, C*H*), 0.28, 0.14 (s, $SiCH_3$). $^1H$ NMR ($CDCl_3$) δ (ppm) 8.54, 8.36, 8.21 (s, C*H*), 0.41, 0.32, 0.23, 0.15 (s, $SiCH_3$). Integrations give satisfactory peak intensity ratios in both solvents. In benzene, the compound exists solely as the "symmetric" isomer **4A** while in chloroform a mixture of the "symmetric" isomer **4A** and the "asymmetric" isomer **4B** is observed.

**Preparation of $[HCN_2S_2]_2$ (2, R = H, E = S).** A solution of *N,N,N'*-tris(trimethylsilyl)formamidine (**3**, 13.0 g, 50 mmol) in 20 mL of $CH_2Cl_2$ was added slowly to a solution of excess sulfur dichloride in 100 mL of $CH_3CN$. The mixture was stirred at room temperature for 30 min and then filtered to afford crude 1,2,3,5-dithiadiazolium chloride (**5**, E = S) as a pale-yellow powder (5.4 g, 38 mol, 77%). Reduction of this yellow solid (2.76 g, 19.6 mmol) with triphenylantimony (4.0 g, 11 mmol) in 20 mL of $SO_2$(l) followed by solvent removal and sublimation of the residual solid at 40 °C/$10^{-2}$ Torr afforded black needles of $[HCN_2S_2]_2$ (**2**, R = H, E = S) (1.82 g, 88%), mp 98–100 °C. MS (70 eV) *m/e* 105 ($M^+$, 65%), 78 ($S_2N^+$, 100%), 64 ($S_2^+$, 15%), 59 ($HCNS^+$, 35%), 46 ($NS^+$, 45%). IR (1600–250 region, Nujol mull) 1235 (sh), 1214 (m, br), 898 (w), 825 (m), 780 (m), 742 (vs), 504 (s), 498 (s), 449 (w) $cm^{-1}$. Anal. Calcd for $HCN_2S_2$: C, 11.40; H, 0.96; N, 26.64. Found: C, 11.54; H, 1.13; N, 26.48. Samples of the dimer suitable for X-ray work were grown by sublimation at 70 °C/760 Torr (argon). A sample of dimer was placed in a 25 cm long sealed (under argon) glass tube (25 mm o.d.) which was heated so as to generate a steady temperature gradient from one end (at 70 °C) to the other (at ambient temperature). Blue-black needles formed at the cool end over a period of several days.

**Preparation of $[HCN_2Se_2]_2$ (2, R = H, E = Se).** A solution of *N,N,N'*-tris(trimethylsilyl)formamidine (**3**, 6.38 g, 24 mmol) in 20 mL of $CH_2Cl_2$ was added dropwise to a solution of selenium dichloride (3.60 g, 24 mmol, prepared *in situ* from Se and $SeCl_4$) in 140 mL of acetonitrile. The mixture was stirred at room temperature for 30 min and then filtered to afford crude 1,2,3,5-diselenadiazolium chloride (**5**, E = Se) as a red-brown powder (5.1 g, 22 mol, 89%). Reduction of this crude salt (1.27 g, 5.4 mmol) with triphenylantimony (0.96 g, 2.7 mmol) in 20 mL of acetonitrile yielded the dimer **2** (R = H, E = Se), which was purified by sublimation at 50 °C/$10^{-3}$ Torr as lustrous grey-black needles (0.56 g, 52%); dec > 100 °C. MS (70 eV) *m/e* 201 ($M^+$, 40%), 174 ($Se_2N^+$, 95%), 160 ($Se_2^+$, 100%), 107 ($HCNSe^+$, 8%), 94 ($SeN^+$, 20%), 80 ($Se^+$, 50%). IR (1600–250 region, Nujol mull) 1246 (m), 901 (w), 795 (m), 721 (m), 623 (s), 588 (w), 559 (vs), 485 (w), 475 (s), 323 (vs) $cm^{-1}$. Anal. Calcd for $HCN_2Se_2$: C, 6.04; H, 0.51; N, 14.08. Found: C, 6.19; H, 0.53; N, 14.27. The ESR spectrum (in $CH_2Cl_2$, 295 K) of **1** (E = Se, R = H) consists of a very broad featureless singlet with $g = 2.0409$.

**X-ray Measurements.** All X-ray data were collected on an ENRAF-Nonius CAD-4 diffractometer with monochromated Mo Kα (λ = 0.71073 Å) radiation. Crystals of the dimer **2** (R = H, E = S) were mounted in glass capillaries. Data were collected using a $\theta/2\theta$ technique. The structure was solved using direct methods and refined by full-matrix least squares which minimized $\sum w(\Delta F)^2$. A summary of crystallographic data is provided in Table IX. The crystals readily twin; the data set used for this report is one of five complete data sets collected from five different crystals. The crystal chosen for data analysis/solution showed, as did the others, a systematic anomalous behavior in two specific regions of data: $-3,k,l$ ($R = 0.55$) and $-6,k,-l$ ($R = 0.52$), where the numerous reflections with high $\Delta F$ all have $F_{obs} \gg F_{calcd}$. The relationship between the reciprocal lattices of the twin components was revealed by zero and upper layer Weissenberg photographs and explains lattice overlaps at $h = 3$ and 6. Thus 218 (out of 1875) reflections with $I > 3\sigma(I)$ were given zero weight in the refinement. In addition, the intensities of the $0kl$ reflections were multiplied by 0.8 to correct for the extra intensity contributed to those reflections by the minor twin component. This factor of 0.8 is consistent with the relative intensities of the two lattices, as shown by the films. Hydrogen atoms were idealized in planar orientations at a C–H bond length of 0.95 Å. Data collection, structure solution, and refinement parameters are available as supplementary material.

(21) Von Niessen, W.; Schirmer, J.; Cederbaum, L. S. *J. Chem. Soc., Faraday Trans. 2*, **1986**, *82*, 1489.

(22) Brauer, G. *Handbook of Preparative Chemistry*; Academic Press: New York, 1963; Vol. 1, p 423.

Table IX. Crystal Data for 2 (R = H, E = S)

| | |
|---|---|
| formula | $S_4N_4C_2H_2$ |
| fw | 210.30 |
| $a$, Å | 6.833(6) |
| $b$, Å | 16.463(4) |
| $c$, Å | 19.161(4) |
| $\beta$, deg | 93.57(4) |
| $V$, Å$^3$ | 2151(2) |
| d(calcd), g cm$^{-3}$ | 1.95 |
| space group | $P2_1/n$ |
| $Z$ | 12 |
| λ, A | 0.710 73 |
| temp, K | 293 |
| $\mu$, mm$^{-1}$ | 1.20 |
| $R(F^2)$, $R_w(F^2)$[a] | 0.057, 0.080 |

[a] $R = [\sum\|F_o| - |F_c\|]/[\sum|F_o|]$; $R_w = \{[\sum w\|F_o| - |F_c\|^2]/[\sum(w|F_o|^2)]\}^{1/2}$.

**ESR Spectra.** ESR spectra were recorded on a Varian E-109 spectrometer (at Guelph) and a home-built instrument (at AT&T Bell Labs). The microwave bridge used in the AT&T experiments is of conventional homodyne design, using a voltage-tunable Gunn diode source (M/A-COM MA87840) and a Varian V-4531 X-band cavity with an LTR-3 liquid He dewar assembly (APD Cryogenics). A PAR 5210 lock-in amplifier served as modulation source and signal detector, and a 5209 was used for automatic frequency control. This instrumentation was interfaced to a PC for data acquisition and analysis. The magnetic field was controlled by a Varian V-FR2503 Field-Dial unit modified for sweeping by a computer-generated ramp. Field calibrations were made with either a tracking NMR fluxmeter or a DTM-141D Teslameter (GMW Associates), and frequency measurements, with an HP-5350B counter. Samples to be analyzed were dissolved in toluene degassed by several freeze–pump–thaw cycles. Simulations of powder pattern spectra were performed with the program QPOWA,[23] compiled with the NDP 4.0.2 FORTRAN compiler, and implemented on a 486/50 MHz PC.

**Infrared Spectra.** Mid-infrared spectra for 1 (R = H, E = S) were obtained on a Nicolet 20SXC interferometer using a 20-cm gas cell with KBr windows. Resolution was 1 cm$^{-1}$, and 1000 scans were coadded. Nujol mull spectra for 2 (R = H; E = S, Se) were obtained on the same instrument, but at 2 cm$^{-1}$ resolution and with CsI windows.

**UV Photoelectron Spectra.** PE spectra of 1 (E = S, Se; R = H) were recorded on a photoelectron spectrometer constructed using components supplied by Comstock, Inc.[24] These included a mean 4-in. hemispherical energy analyzer in conjunction with chevronned 50-mm microchannel plates acting as a position-sensitive detector. Readout was by means of a resistive anode. This instrument, described elsewhere,[25] provides a kinetic energy bite of 20% of the transmission energy. The spectra shown in Figure 6 were recorded with a transmission energy of 20 eV, giving a resolution of 60 meV and an energy bite of 4 eV. In each case four overlapping windows of data were collected, linearized, normalized, and assembled using LOTUS 1-2-3. Spectra were recorded for the gas-phase species obtained as the volatile products from the respective solid dimers. The low volatility of the selenium compound necessitated recording spectra at 2.1 × 10$^{-6}$ Torr, as measured below the analyzer, essentially the lowest limit for this instrument, and hence the signal-to-noise ratio is inferior to that for the sulfur compound. 30 000 scans were obtained for the sulfur compound and 90 000 for the selenium analog. Spectra were calibrated using MeI and Ar.

***Ab Initio* Computational Methods.** *Ab initio* calculations were carried out with the GAUSSIAN90[26] and GAUSSIAN92[27] program systems. Unrestricted Hartree–Fock calculations for the doublet radicals had $S^2$ values in the range 0.9–1.0, indicating significant amounts of spin contamination. Additional restricted open-shell calculations were performed on the S radical with the 3-21G* and 6-31G* basis sets and for the Se radical at the 3-21G* level. References for the basis sets may be found in the Gaussian92 User's Guide[28] except for the Se 3-21G* set taken from Hehre and Dobbs[29] and the CEP-31G basis for Se.[30] Values of the d function exponents were taken as follows: S, 0.54 CEP31G* and LANL1DZ*; Se, 0.370 LANL1DZ* and CEP31G* and 0.338 3-21G*. Geometries of both the radicals and dimers were optimized using gradient methods, but with a restriction to $C_{2v}$ symmetry. In addition, for the dimers, the two rings were held planar and parallel. Harmonic vibrational frequency analyses reveal that at the highest levels, 3-21G* (Se) and 6-31G** (S), the radicals are minima (all real vibrational frequencies). The sulfur dimer was also a minimum at the 3-21G* SCF level while the selenium dimer had one small imaginary frequency (54$i$ cm$^{-1}$). In determining the binding energies, electron correlation effects were considered through Møller–Plesset perturbation theory (MP2, MP3, MP4SDQ) calculations on the SCF optimized structures.

**Acknowledgment.** Financial support was provided at Guelph by the Natural Sciences and Engineering Research Council of Canada (NSERC) and at Arkansas by the National Science Foundation (EPSCOR program). C.D.B. acknowledges a DOE/ASTA Traineeship.

**Supplementary Material Available:** Tables of crystal data, structure solution and refinement, atomic coordinates, bond lengths and angles, anisotropic thermal parameters, and ORTEP drawings of the asymmetric unit for 2 (R = H, E = S) (6 pages); observed and calculated structure factors for the monoclinic phase of 2 (20 pages). Ordering information is given on any current masthead page.

(23) (a) Nilges, M. J. Ph.D. Thesis, University of Illinois, Urbana, Illinois, 1979. (b) Belford, R. L.; Nilges, M. J. Computer Simulation of Powder Spectra. EPR Symposium, 21st Rocky Mountain Conference, Denver, Colorado, 1979. (c) Maurice, A. M. Ph.D. Thesis, University of Illinois, Urbana, Illinois, 1980.

(24) Comstock, Inc., Oak Ridge, TN.

(25) Alaee, M.; de Laat, R. H.; Westwood, N. P. C. To be published.

(26) Frisch, M. J.; Head-Gordon, M.; Trucks, G. W.; Foresman, J. B.; Schlegel, H. B.; Raghavachari, K.; Robb, M. A.; Binkley, J. S.; Gonzalez, C.; Defrees, D. J.; Fox, D. J.; Whiteside, R. A.; Seeger, R.; Melius, C. F.; Baker, J.; Martin, R. L.; Kahn, L. R.; Stewart, J. J. P.; Topiol, S.; Pople, J. A. *GAUSSIAN90*; Gaussian, Inc.: Pittsburgh, PA, 1990.

(27) Frisch, M. J.; Trucks, G. W.; Head-Gordon, M.; Gill, P. M. W.; Wong, M. W.; Foresman, J. B.; Johnson, B. G.; Schlegel, H. B.; Robb, M. A.; Replogle, E. S.; Gomperts, R.; Andres, J. L.; Raghavachari, K.; Binkley, J. S.; Gonzalez, C.; Martin, R. L.; Fox, D. J.; Defrees, D.; Baker, J.; Stewart, J. J. P.; Pople, J. A. *GAUSSIAN92*, Revision A; Gaussian, Inc.: Pittsburgh, PA, 1992.

(28) Frisch, M.; Foresman, J.; Frisch, A. *Gaussian 92 User's Guide*; Gaussian, Inc.: Pittsburgh, PA, 1992.

(29) Dobbs, K. D.; Hehre, W. J. *J. Comput. Chem.* **1986**, *7*, 359.

(30) Jaisen, P. G.; Stevens, W. J. *J. Chem. Phys.* **1985**, *83*, 2984.